Nuclear Inst. and Methods in Physics Research, A 1029 (2022) 166470

Contents lists available at ScienceDirect

Nuclear Inst. and Methods in Physics Research, A

journal homepage: www.elsevier.com/locate/nima

Fiber optic sensors in the ATLAS Inner Detector

L. Scherino [a,b,*], E.J. Schioppa [a,c,d], A. Arapova [e], G.M. Berruti [b], W.J. Bock [e], A. Boniello [b], A. Borriello [f], S. Campopiano [g], M. Consales [b], A. Cusano [b], F. Esposito [g], A. Iadicicco [g], S. Kachiguine [h], P. Mikulic [e], K. Nagai [i], T. Neves [a,j], P. Petagna [a], G. Quero [b], D. Robinson [k], A. Srivastava [g], P. Vaiano [b], N. Venturi [a], M. Zarrelli [f], A. Zotti [f], S. Zuppolini [f]

[a] CERN, the European Organization for Nuclear Research, Esplanade des Particules 1, 1211 Geneva, Switzerland
[b] University of Sannio, Department of Engineering, Optoelectronics Group, I-82100 Benevento, Italy
[c] Università del Salento, Dipartimento di Matematica e Fisica "E. De Giorgi", via per Arnesano, 73100 Lecce, Italy
[d] INFN, Istituto Nazionale di Fisica Nucleare, sezione di Lecce, Italy
[e] Photonics Research Center, Université du Québec en Outaouais, rue 101 St-Jean Bosco, Gatineau, Québec, J8X3G5, Canada
[f] Institute for Polymers, Composites and Biomaterials (IPCB) - National Research Council, I-80055 Portici, Italy
[g] Department of Engineering, University of Naples "Parthenope", Centro Direzionale Isola C4, 80143, Napoli, Italy
[h] University of California, Santa Cruz, USA
[i] University of Oxford, Department of Physics, Oxford, UK
[j] EPFL, Echole Polytechnique Federale de Lausanne, Lausanne, Switzerland
[k] Cavendish Laboratory, Cambridge University, Cambridge, UK

ARTICLE INFO

Keywords:
Fiber optic sensor
Radiation hardness
Long period grating
Environmental monitoring
High energy physics

ABSTRACT

A prototype system of Fiber Optic Sensors (FOS) for the accurate measurement of temperature and relative humidity, has been installed inside the Inner Detector volume of the ATLAS experiment at the LHC. The goal is to evaluate the behavior of the technology against radiation effects, and possibly to assess its suitability for future collider experiments, starting from HL-LHC. It follows the description of the work that has led to the choice of the sensors, their testing and calibration in the laboratory, their successive installation and operation in ATLAS, and the development of the data acquisition chain. The first results on performance are reported.

1. Introduction

The design, development, construction and operation of particle detectors at colliders is becoming more and more demanding and complex. Such experiments require performing instruments to cope with the ever increasing luminosity of the accelerators. One of the main concerns when designing particle detectors for future collider experiments, is their resistance to radiation damage. This impacts both the sensitive parts of the detectors (the actual particle sensors) and the infrastructure surrounding them at any level, be it the readout electronics, the structural materials or other components that ensure the correct functioning of the full apparatus. In this category, one includes all the sensors that are employed to monitor the environmental conditions of the detector, especially those that are installed close to the collision region, where the levels of radiation are the highest.

Particular attention has been recently devoted to the study of possible radiation hard solutions for monitoring temperature (T) and relative humidity (RH) in the central regions of future collider experiments. This is especially important, because normally these regions are equipped with delicate particle trackers based on semiconductor detectors, which must be operated in very controlled environmental conditions. In order to minimize junction leakage currents, these detectors are usually operated at low temperatures and inside a sealed volume which is flushed with dry gas mixtures. However, the risk of water contamination must always be considered. Therefore, constant monitoring of the dew point is crucial, as water condensation may cause irreversible damages (see for example [5]).

For this reason, the environment in which these detectors live need to be constantly monitored for temperature and humidity. In fact, such detectors are provided with an extensive number of sensors which, at the same time, have to face the challenge of surviving to high radiation levels. While conventional sensors have shown sufficient radiation tolerance at the Large Hadron Collider (LHC), and might be still suitable for the High Luminosity LHC (HL-LHC).[1] their employment in future collider experiment is questionable, as they will most likely not survive the increased radiation levels. New technologies are thus essential (for more details see Chapter 1 of [6]).

* Corresponding author at: CERN, the European Organization for Nuclear Research, Esplanade des Particules 1, 1211 Geneva, Switzerland.
E-mail address: lorenzo.scherino@cern.ch (L. Scherino).

[1] For example, lifetime radiation fluences of $\mathcal{O}\left(10^{14-17}\right)$ Si 1 MeV n_{eq}/cm^2 and $\mathcal{O}\left(10^{4-7}\right)$ Gy are foreseen in the ATLAS Inner Tracker (ITk) in the detector depending on the distance from the collision point [1–4].

https://doi.org/10.1016/j.nima.2022.166470
Received 9 April 2021; Received in revised form 24 January 2022; Accepted 3 February 2022
Available online 15 February 2022
0168-9002/© 2022 The Author(s). Published by Elsevier B.V. This is an open access article under the CC BY license (http://creativecommons.org/licenses/by/4.0/).

In this context, Fiber Optic Sensors (FOS) are of particular interest for high energy physics applications not only because there is clear evidence of their radiation tolerance [7–11], but also because they naturally comply with the typical requirements for operation inside the volume of a collider particle detector. Among the other features, they are non-electrical devices, which means there is no need for a power supply in the measuring area, they have a low invasiveness because they are small and light (which is crucial for installation inside particle trackers), they can offer complete immunity to electromagnetic interference. Additionally, they allow for multipoint or distributed measurements on the same optical fiber and for measuring different environmental parameters at the same time.

The first infield application of FOS for monitoring relative humidity in high radiation environments, was carried out in the cold areas of Tracker Bulkhead of the Compact Muon Solenoid (CMS) experiment [12], with the installation of a network of 72 thermo-hygrometers [13]. In this paper we present the first installation in the Inner Detector of the ATLAS experiment, of novel thermo-hygrometers based on improved FOS technology.

2. FOS technology

FOS technology is divided into two macro-categories: point sensors, such as grating-based sensors, and distributed fiber optic sensors (DFOS), in which the entire length of the fiber can be used as a sensing element. In this work, we focused on grating-based point sensors. These are based on the periodic perturbation of the refractive index of the optical fiber core over a portion of its length. This category of sensors falls into two general classifications based on the grating period: Fiber Bragg Gratings (FBGs) have typically a period of the order of submicron and Long Period Gratings (LPGs) have a period from 100 μm to 1 mm. Both sensors are generally sensitive to temperature and/or strain (and the refractive index of the external medium in the case of LPGs), in which case they are referred to as "bare". However, they can also be made sensitive to RH if a proper layer of hygroscopic material is applied, in which case they are called "coated".

As demonstrated by the FOS installed in the CMS experiment, FBGs present a few limitations: low sensitivity to humidity at low RH levels and cross-sensitivity of coated FBGs to both temperature and humidity. Moreover, coated FBGs are produced with a layer of polymeric materials, which influence the triggering of the sensing mechanism and which are affected by aging. In order to overcome these limitations, a new generation of humidity monitoring sensors based on LPGs coated with Titanium Dioxide (TiO_2), rather than polymers, has been developed.

2.1. Long Period Grating technology

Long Period Fiber Gratings (LPFGs or LPGs) are photonic devices realized by inducing a periodic refractive index modulation of the core (sometimes also of the cladding) of a single mode optical fiber along a small section of its length [14]. The typical length of these devices is in the order of centimeters (typically 2–3 cm). The period of the sensitive pattern is in the order of hundreds of micrometers (typically Λ = 100-500 μm). This periodic modulation allows for the transfer of power from the fundamental guided core mode to discrete forward-propagating cladding modes at a distinct wavelength for each of them, where the so-called phase matching condition is satisfied:

$$\lambda_{res,j} = (n_{eff,co} - n^j_{eff,cl}) * \Lambda \tag{1}$$

Here, $n_{eff,co}$ is the effective refractive index of the core, $n^j_{eff,cl}$ represents the effective refractive index of the jth cladding mode and Λ is the period of the grating. As a result, the transmitted spectrum will have attenuation bands that arise from light coupling from the guided mode to the cladding mode. Part of the electromagnetic field of the cladding modes, that propagates as evanescent waves in the surrounding medium, makes the effective refractive index of the cladding sensitive to the conditions (e.g. temperature) of the surrounding environment.

2.2. LPG Sensing Principles

The sensitivity of LPGs to temperature depends on three factors: the period of the LPG, the order of the cladding mode and the composition of the optical fiber [15]. The differentiation of Eq. (1), with respect the temperature, yields to:

$$\frac{d\lambda_{res,j}}{dT} = \Lambda\left(\frac{dn_{eff,co}}{dT} - \frac{dn^j_{eff,cl}}{dT}\right) + \left(n_{eff,co} - n^j_{eff,cl}\right)\frac{d\Lambda}{dT} \tag{2}$$

Using the chain rule on Eq. (2), the most common form of the temperature sensitivity is obtained:

$$\frac{d\lambda_{res,j}}{dT} = \frac{d\lambda_{res,j}}{d\left(\delta n_{eff}\right)}\left(\frac{dn_{eff,co}}{dT} - \frac{dn^j_{eff,cl}}{dT}\right) + \Lambda\frac{d\lambda_{res,j}}{d\Lambda}\frac{1}{L}\frac{dL}{dT} \tag{3}$$

where, $\frac{1}{\Lambda}\frac{d\Lambda}{dT} = \frac{1}{L}\frac{dL}{dT}$, L is the length of the LPG and δn_{eff} represents the difference between $n_{eff,co}$ and $n^j_{eff,cl}$. The first term of Eq. (3) describes the actual thermo-optical effect, while the second term is commonly called the waveguide contribution, and represents the variation of the grating periodicity of the LPG as a function of temperature [16].

Compared to FBGs, LPGs provide higher sensitivities in measuring the two parameters that can be sensed (i.e. temperature and strain). Furthermore, the refractive index sensitivity of LPGs has enabled the development of the optical hygrometers based on metal-oxides, rather than polymers, as coating material. In particular, titanium dioxide (TiO_2) is an excellent candidate due to its hygrosensitive characteristics and high refractive index (n = 1.96). It has been demonstrated that integrating a layer of titanium dioxide (TiO_2) on the LPGs, the absorption/desorption of water in the hygrosensitive coating produces a change of the refractive index (and thickness). This creates a spectral and amplitude variation in the LPG attenuation bands, independent of the adhesion properties of the coating to the grating itself [17]. Typically, the change of the attenuation band of the jth cladding mode, following a change in RH, is a nonlinear function, and the sensitivity to humidity is from one to three orders of magnitude higher than that exhibited by FBG-based RH sensors, especially at very low humidity values [8].

2.3. Radiation tolerance

The effects of radiation on optical fiber devices and optical fibers in general have been widely studied over the years. A number of reviews have appeared in literature, which summarize the results and status. For example, Girard [18] gives an overview of the main fiber-optic technologies that are used in a variety of applications, also of interest in harsh environments (including point sensors, such as FBG and LPG). Despite the wealth of research that has been done, it is difficult to define a universal classification of the response of fiber optic sensors following exposure to ionized radiation, as this response depends on multiple factors such as the manufacturing parameters of the sensor itself and the parameters of the radiation source (e.g. type, energy) [19]. This means that, when choosing the specific technology to be employed in a hard radiation environment, one must rely on results obtained on that very technology. Such a selection process has been followed for the choice of sensors employed in this work. While the FBG samples have been simply inherited from the previous experience in CMS, the choice of LPG sensors, which had never been employed at the LHC before, has been guided by a number of previous results (see for example [7]).

3. Choice of LPG sensors

Several LPGs were selected for this project, produced in-house with three different fabrication techniques: UV-induced LPGs inscription, arc-induced LPGs and femtosecond laser pulses LPGs. The first method

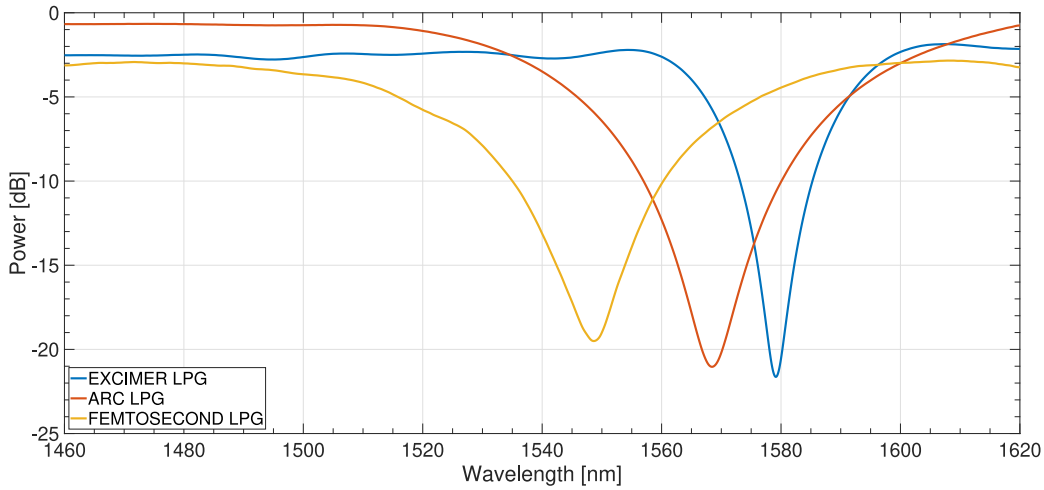

Fig. 1. Example of spectra of the three types of LPG used.

is based on the phenomenon of photosensitivity and allows the grating to be written by exposing the fiber to an ultraviolet laser source. These LPGs have been inscribed in a photosensitive single-mode B-Ge co-doped optical fiber (Fibercore PS1250/1500[2]), through a point-to-point technique, using a KrF pulsed excimer laser (LightBench 1000, Optec, Belgium[3]) operating at a wavelength of 248 nm. We will refer to these sensors as "EX" LPGs. On the contrary, the other two manufacturing methods are non-photosensitive. Arc-induced LPGs are realized by creating a physical periodic deformation of the fiber by means of an electrical discharge while a longitudinal force is applied. Finally, LPGs produced through the femtosecond laser are based on the densification of the glass in order to create a periodic variation of the refractive index of the optical fiber. These sensors will be called respectively "ARC" and "FS" LPGs. ARC and FS gratings are fabricated in pure-silica core fibers, using a S1310-MTA from Nufern.[4] Examples of spectra of three LPG sensors, made with the three fabrication techniques, are shown in Fig. 1.

Through the use of different manufacturing techniques, it is possible to have a direct comparison of performance, in terms of temperature and humidity detection, insensitivity to polarization and radiation resistance. For each point of installation in the ATLAS Inner Detector, a pair of sensors (bare and coated) has been installed for each type of manufacturing technique.

3.1. Coating

In order to deposit TiO_2 onto the fiber, sol–gel deposition technique has been selected for its numerous advantages in terms of good optical quality and low loss, ring shaped symmetry, and adequate longitudinal uniformity over the grating length [17,20]. Such deposition technique, which was optimized for this application, was previously demonstrated to guarantee smoothness and homogeneity of the LPG overlay and it was found to assure good performance of the final device in terms of RH detection [17].

3.2. Radiation tolerance

A number of studies have proven the resistance to radiation of the selected LPGs. Thorough investigations are being carried out since 2011, in order to study the behavior of the LPGs under the exposure to radiation sources of different types, probing different technologies under different conditions. The first evidence of radiation tolerance of LPG sensors coated with a 100 nm TiO_2 layer, written by UV laser fabrication technique for RH monitoring at temperatures below 0 °C was obtained around 2014 [17]. In that work, a sensor was exposed to a 10 kGy dose of ionizing gamma radiation, which resulted in no sensible modification of the sensitivity to RH. Further measurements have been carried out on uncoated LPGs inscribed on B-Ge co-doped optical fibers by a UV laser source and exposed to high fluences of protons [9]. The samples were exposed to a proton source of 4.4×10^{15} p/cm^2 accumulating a total dose of 1.16 MGy. Following exposure, the samples showed a resonance wavelength red shift and an attenuation of the visibility, however they were still operational, demonstrating their tolerance to these radiation levels. In order to explain the observed behavior after irradiation, several numerical studies were carried out. At the same time, Esposito et al. conducted several irradiation campaigns on arc-induced LPGs in different fibers. They focused on the exposure of the sensors first under gamma radiation and then under neutron-gamma radiation. In the first campaign, they used a ^{60}Co source at the "Horia Hulubei" institute (Măgurele, Romania), to expose arc-induced LPG, written on different types of standard fibers, to a final dose up to 35 kGy achieved at a doserate of 0.2 kGy/h [10,11,21,22]. The authors showed a red shift in the resonance wavelength of the samples as the dose increased up to 15 kGy. Above this value, they observed that this effect saturates. Also in this case, numerical simulations were performed in order to understand the post-irradiation behavior, and the change in temperature sensitivity observed in some of the sensors. Another campaign on arc-induced LPGs was conducted at the TRIGA research nuclear reactor of the Nuclear Research Institute ICN (Mioveni, Romania) [23]. The samples were exposed to a neutron-gamma source, achieving a dose of 64.8 kGy at a rate of 9 Gy/s and a neutron flux of 1.25×10^{12} n/cm^{2}s reaching a fluence of 9.18×10^{15} n/cm^2. Also in this case the authors first observed a red shift in the wavelength of the samples up to a dose of about 16 kGy and a neutron fluence of 2.3×10^{15} n/cm^2, after which the sensor response saturated, demonstrating perfect agreement with the previous ^{60}Co campaign. While these results are very promising, such studies are not yet complete and are therefore still ongoing. Proton, neutron and gamma irradiation campaigns are being carried out in order to study the effects of different radiation sources on the response of the sensors and to understand the factors that most influence it.

3.3. Package

The sensitive section of the FOS consists of a fragile optical fiber (bare or coated), which is highly prone to mechanical damage. In order to protect the sensor, a package has been developed, based on a ceramic

[2] https://fibercore.humaneticsgroup.com/products/photosensitive-fiber/boron-doped-photosensitive-fiber/ps12501500 .

[3] https://optec-laser-systems.com/ .

[4] https://content.coherent.com/pdf/s1310_p_spec_202011122144.pdf .

Fig. 2. FOS package.

perforated tube with copper extremities (Fig. 2), in which the LPG is hosted. Furthermore, since LPG-based sensors require a pre-strain in order to function correctly, the task of the package is also to maintain the sensor under a certain pre-strain. In this case, the pre-strain was ensured by pulling the fiber using a 30 g weight during the packaging procedure.

4. Laboratory tests and results

Prior to installation in ATLAS, the selected FOS underwent an extensive testing campaign in the laboratory.

4.1. Experimental setup for T and RH characterization

To characterize thermo-hygrometric sensors based on LPG platform, it is important to test them in an environment with accurate temperature and humidity settings. Specifically, we need to work at very low RH levels (less than 10% RH), controlling relative humidity and temperature variations with high accuracy. Climatic chambers providing such performance were not available on the market, or had prohibitive costs. For this reason, a custom climatic chamber, made in Aluminium and insulated from the external environment through a hermetic polystyrene box, has been developed and manufactured in the Experimental Physics-Detector Technology (EP-DT) group at CERN. A picture of the chamber is shown in Fig. 3, left. The setup is equipped with a temperature control circuit (Julabo FP-50[5]) to control the temperature over a wide range. In addition, a circuit of copper insulated pipes is present, which is connected to two electrical valves (Bronkhorst El-Flow[6]) The valves allow us to reach the required humidity level by mixing different amounts of dry and wet air, that are injected directly into the climatic chamber (Fig. 3, right). In this way, we are able to control the relative humidity variations inside the climatic chamber with a resolution of 0.1% RH in a range from 0% RH up to 90% RH. The temperature range that the climatic chamber can reach is from −20 °C up to 50 °C.

The compressed air inside the circuit is first dried and then injected into the setup described above. From here, moisture is generated in a bubbler containing water in a controlled manner. A high-performance Chilled Mirror Dew Point Hygrometer (EdgeTech DewMaster) is used as a reference sensor for the measurement of moisture. Inside the chamber, three additional commercial electronic hygrometers (Honeywell HIH-4000 Series) are installed, together with three calibrated resistive thermometers (PT100) for temperature reference. These sensors interface with the outside through Fischer hermetic connectors. The control software of this setup is implemented in a LabVIEW VI, which also saves all the data for posterior analysis.

As far as the interfacing to the outside of the FOS is concerned, the system provides four ultra-vacuum feedthroughs with sixteen channels of FC/APC adapters. The sensors are connected to an accurate optical interrogator[7] (Micron Optics HYPERION Optical Sensing Instrument si155), characterized by a resolution of 1 pm and an operating wavelength range from 1460 nm to 1620 nm.

4.2. Calibration

In order to calibrate the sensors based on LPG platform, characterizations in temperature (in the −5 ° C – 25 ° C range) and relative humidity (in the 0%–25% range) have been carried out using the setup described in Section 4.1.

4.2.1. Temperature calibration

In order to characterize all LPG devices in temperature, it was decided to keep the relative humidity level constant, at a value of 10% ± 1% RH, to avoid cross-sensitivity problems.

In order to calibrate all the devices, several temperature tests have been performed. The sensor response has been acquired while the temperature was changed from 25 °C to −5 °C. An example of T and RH values measured by the reference electric sensors during one of these tests is shown in Fig. 4. Figs. 5–7 shows the response of the LPG sensors during temperature calibration. All sensors showed a linear behavior in the investigated temperature range, except for the femto bare (Fig. 6) and arc bare (Fig. 7) sensors, which showed unexpected spectral changes for temperature lower than 0 °C. Such behavior is probably attributable to fiber bending. Therefore, for these sensors, the calibration points at negative temperature were not considered. This behavior can be explained as an effect of the package. The package not only protects the fiber, but it also keeps it straight in a constant strain state. However, for relatively large temperature variations, the difference in thermal expansion coefficients of the different materials (the copper and ceramic of the package, the glass of the fiber) does not guarantee such strain state. In parallel to this test installation, and for future prototypes, we are conducting further tests at low temperatures (below −30 °C in a commercial climatic chamber) with different packages and different materials.

The temperature sensitivity of each device is calculated as the slope of the characteristic curves shown in Figs. 5, 6, 7. All such values, including the coefficient of determination (R^2), are summarized in Table 1. These results showed that excimer LPG sensors have high temperature sensitivity, high reproducibility and the highest coefficient of determination (R^2). Therefore, it was already clear that they would be the best candidates for the role of reference devices for the other sensors, once installed in the ATLAS Inner Detector.

Since the bare sensors are insensitive to changes in humidity, the total wavelength shift of the attenuation band is uniquely given by the variation of temperature:

$$\Delta\lambda_{\text{total}} = \Delta\lambda_T = S_T \Delta T \tag{4}$$

Therefore, for bare sensors, temperature can be calculated as

$$T_{\text{measured}} = \frac{\lambda_{\text{measured}} - \lambda_0}{S_T} + T_0 \tag{5}$$

where λ_0 indicates the wavelength of the attenuation band when the sensor is measuring at temperature T_0.

[5] https://julabo.us/wp-content/uploads/products/datasheets/JULABO-FP50-MA--9153650.pdf .

[6] https://www.bronkhorst.com/int/products/gas-flow/el-flow-select/?page=1#.

[7] The interrogator is a high speed wide wavelength swept laser source, that allows one to measure a wavelength spectrum with high resolution in a given range.

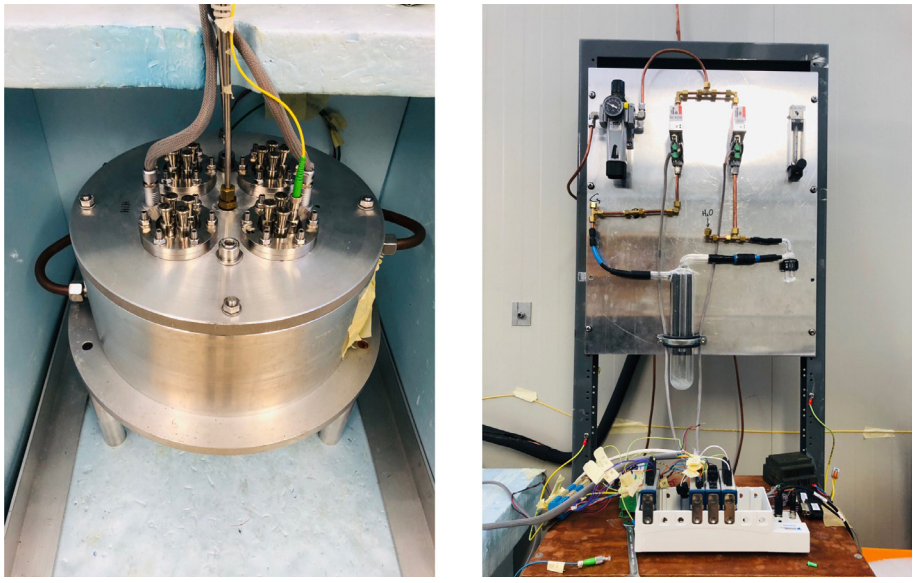

Fig. 3. Two pictures of the laboratory setup. Left: climatic chamber. Right: RH control setup.

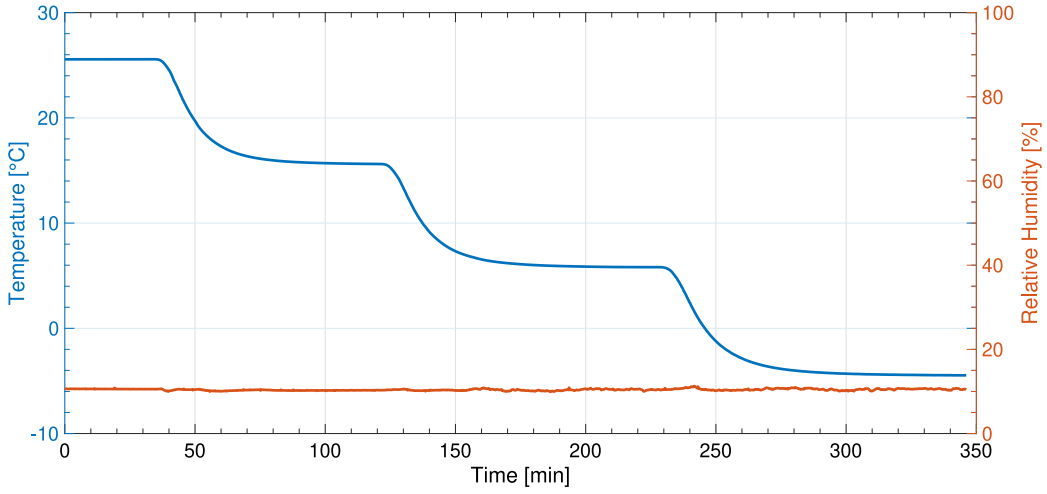

Fig. 4. Climatic chamber conditions as measured by the reference sensors, during temperature calibration.

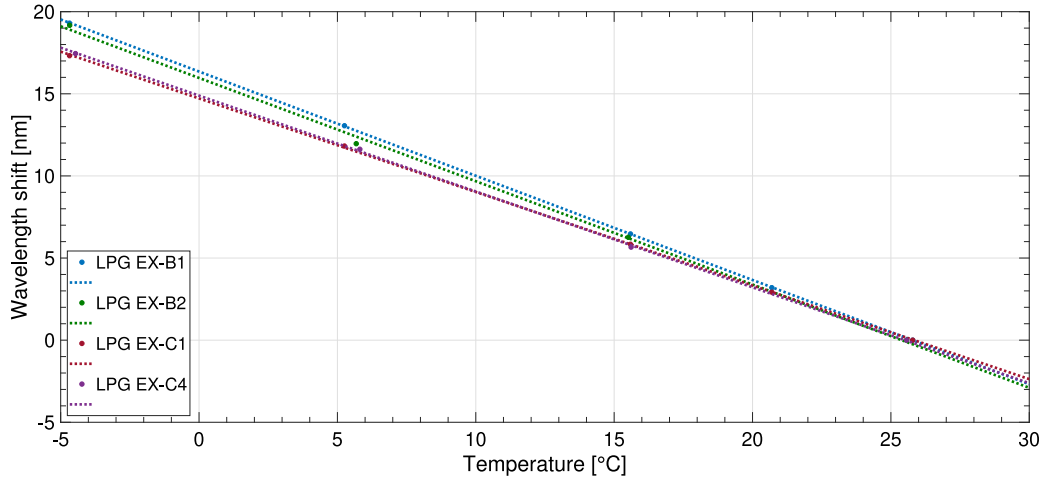

Fig. 5. Temperature calibration curves for the Excimer LPGs.

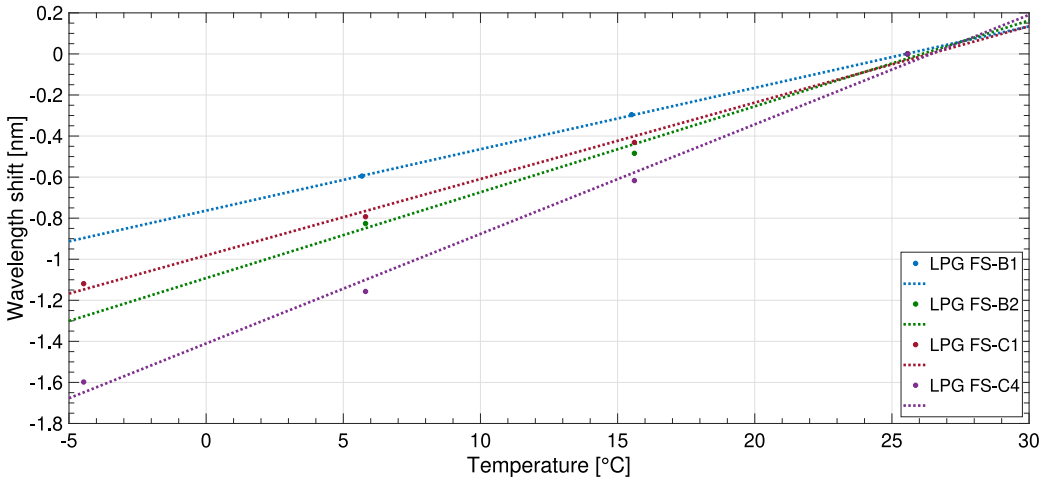

Fig. 6. Temperature calibration curves for the Femto LPGs.

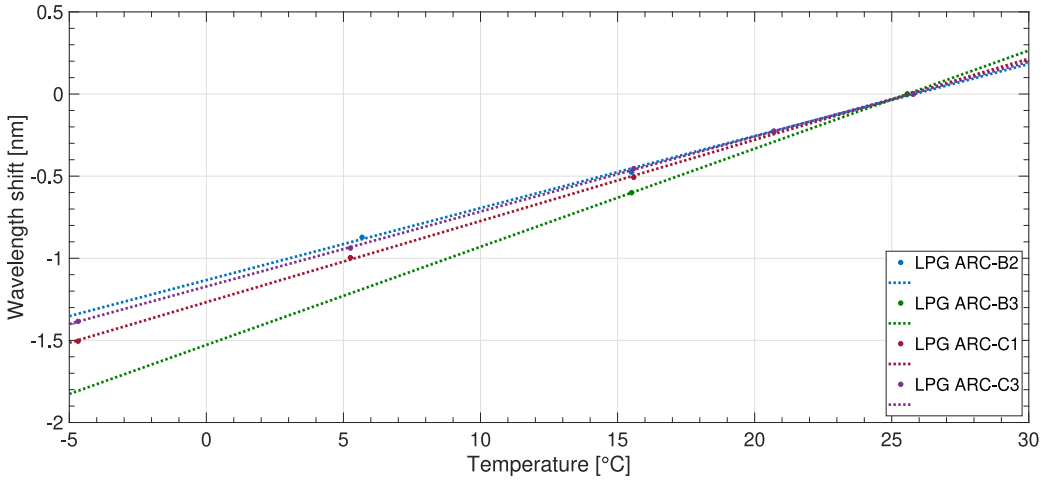

Fig. 7. Temperature calibration curves for the Arc LPGs.

Table 1
List of LPG FOS sensors with the corresponding temperature sensitivities measured in the laboratory. The uncertainties on S_T are the standard errors produced by the maximum likelihood fit. In the last column, R^2 is the coefficient of determination. The sensor with $R^2 = 1$ is the one for which only two calibration points were available, as explained in the text.

Sensor	Type	S_T [nm/°C]	R^2
LPG EX-B1	Bare	−0.634 ± 0.001	0.999
LPG EX-B2	Bare	−0.629 ± 0.016	0.999
LPG EX-C1	Coated	−0.570 ± 0.003	0.999
LPG EX-C4	Coated	−0.584 ± 0.006	0.999
LPG FS-B1	Bare	0.030 ± 0.001	0.999
LPG FS-B2	Bare	0.042 ± 0.004	0.991
LPG FS-C1	Coated	0.037 ± 0.002	0.995
LPG FS-C4	Coated	0.053 ± 0.003	0.993
LPG ARC-B2	Bare	0.044 ± 0.002	0.998
LPG ARC-B3	Bare	0.056 ± 0.001	1
LPG ARC-C1	Coated	0.049 ± 0.001	0.999
LPG ARC-C3	Coated	0.046 ± 0.001	0.999

4.2.2. Relative Humidity Calibration

For the calibration of the coated sensors in relative humidity, this parameter has been varied from 0.2% to 20% at a constant temperature of 25.5 °C. An example of the behavior of RH and T during a test, given by the reference sensors, is shown in Fig. 8. The responses of the coated sensors are presented in Fig. 9, while Fig. 10 shows the RH sensitivities, calculated as the derivative of the response curves.

All sensors show non-linear behavior, with a high slope at low RH levels, according to what was already reported in [8]. At high relative humidity levels (around 25%), the sensitivity of the least sensitive sensor is 0.0045 nm/%RH. This value is comparable with the typical sensitivity of polyimide-coated FBG sensors with thicknesses ranging from 10 μm to 42 μm [24].

All curves in Fig. 10 have been parametrized via a negative logarithmic fit of the form

$$\lambda = a - b * \ln(RH + c) \tag{6}$$

The reason of such a choice is merely practical. In fact, the derivative of Eq. (6), which represents the humidity sensitivity of the sensor, provides a simple analytical form, which can be easily employed to convert wavelength into relative humidity:

$$S_{RH} = \frac{d\lambda}{dRH} = -\frac{b}{c + RH} \tag{7}$$

The analytical expressions for the relative humidity sensitivity are summarized in Table 2.

As a result of the variations in both relative humidity (ΔRH) and temperature (ΔT), the total wavelength shift ($\Delta\lambda$) of the attenuation band of a coated sensor can be expressed as

$$\Delta\lambda_{\text{total}} = \Delta\lambda_{\text{RH}} + \Delta\lambda_T = S_T \Delta T + S_{RH} \Delta RH \tag{8}$$

Combining Eq. (8) with Eq. (5) and (7), it is possible to derive the formula for calculating the relative humidity after temperature

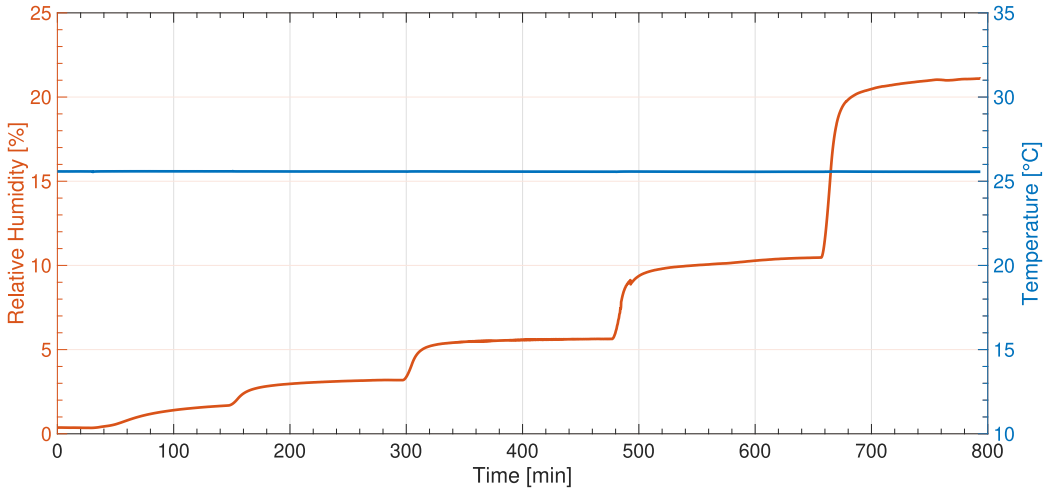

Fig. 8. Climatic chamber conditions as measured by the reference sensors, during relative humidity calibration.

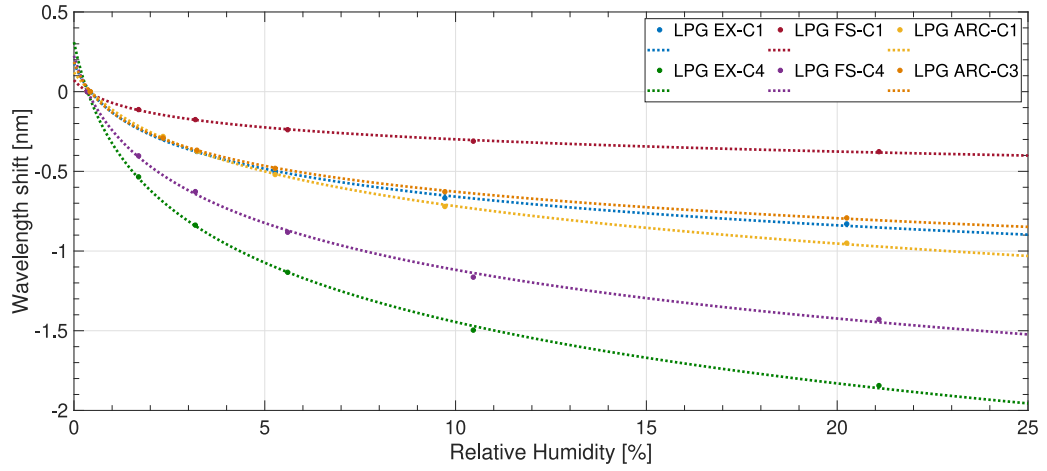

Fig. 9. Responses of the coated sensors.

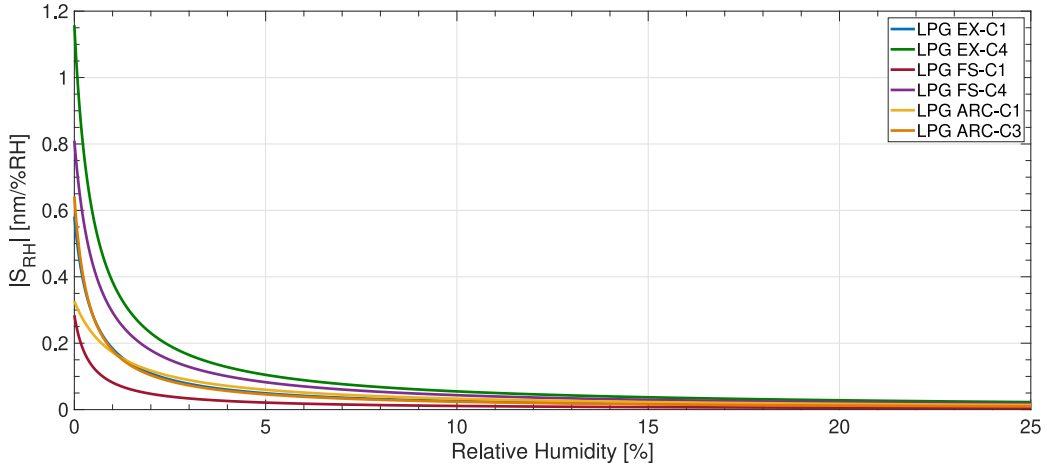

Fig. 10. Sensitivities of the coated sensors.

compensation:

$$RH = \frac{-\frac{\{(\lambda_{\text{measured}}-\lambda_0)-[S_T\times(T_{\text{measured}}-T_0)]\}}{b} * c + RH_0}{1+\frac{\{(\lambda_{\text{measured}}-\lambda_0)-[S_T\times(T_{\text{measured}}-T_0)]\}}{b}} \quad (9)$$

Here λ_0 is the wavelength of the attenuation band of LPG, acquired at T_0 and RH_0, which are given by the reference electrical sensors. The value of T_{measured} is given by the bare LPG sensors, which are only sensitive to temperature.

Fig. 11. The ATLAS Inner Detector End Plate at the time of installation of the Inner Detector, before the sealing panels were mounted.

Table 2
Relative Humidity sensitivities, given according to formula (7). The uncertainties on b and c are the standard errors produced by the maximum likelihood fit.

Sensor	b [nm]	c [% RH]	R^2
LPG EX-C1	0.268 ± 0.014	0.461 ± 0.144	0.998
LPG EX-C4	0.575 ± 0.017	0.496 ± 0.080	0.999
LPG FS-C1	0.114 ± 0.005	0.401 ± 0.106	0.999
LPG FS-C4	0.459 ± 0.021	0.566 ± 0.131	0.999
LPG ARC-C1	0.366 ± 0.012	1.119 ± 0.144	0.999
LPG ARC-C3	0.247 ± 0.006	0.384 ± 0.062	0.999

5. Installation in the ATLAS Inner Detector End Plate

The ATLAS Inner Detector volume represents an ideal workbench to test FOSs for temperature and humidity monitoring in the environment of an actual particle collider experiment. The installation inside the ATLAS Inner Detector volume has been carried out exploiting an intervention that was planned for the end of March 2019 for repair work on the cooling system. Such an intervention foresaw the partial removal of the sealing panels of the Inner Detector End Plates (IDEP) on both side A and side C,[8] leaving sufficient room for installing the FOSs as close as possible to the beam pipe. A picture of the IDEP taken at one side, is shown in Fig. 11.

The prototype FOS system prepared for the installation in ATLAS is made of a total of 19 sensors, consisting of 7 FBG-based and 12 LPG-based sensors. Among the 12 LPGs, 6 are coated with a TiO_2 layer and they are thus sensitive to humidity, while 6 of them are uncoated sensors in order to monitor the temperature level. As for the FBGs, 5 uncoated sensors read the temperature, while the remaining 2 are coated with Polyimide and monitor the humidity level. The sensors have been evenly distributed between side A and side C as summarized in Table 3. Notice that, at each side, 4 LPGs are kept separated while 2 are paired on a single fiber array. The 4 FBGs in side A and the 3 FBGs in side C are also organized in arrays, namely multiple sensors are fabricated on the same optical fiber (see Section 6.1). Such a configuration allows for more than one measurement per readout channel, thus increasing the redundancy of the test system and giving the possibility to test different flavors of each technology, even with a limited number of readout channels.

Table 3
Distribution of the FOS devices installed in the ATLAS IDEP. The 4 FBGs in side A and the 3 FBGs in side C are configured into arrays on single fibers, one per side.

Side	Technology	Sensor	Type	Wavelength[a] [nm]
A	LPG	EX_B1 + EX_C1	Bare, coated	1578, 1501
A	LPG	FS_B2	Bare	1564
A	LPG	FS_C4	Coated	1548
A	LPG	ARC_B2	Bare	1568
A	LPG	ARC_C1	Coated	1574
A	FBG	UV MO, irradiated	Bare	1512
A	FBG	UV Welltech, irradiated	Coated	1564
A	FBG	FS Fibertech, irradiated	Bare	1550
A	FBG	FS Fibercore	Bare	1545
C	LPG	EX_B2 + FS_C1	Bare, coated	1582, 1532
C	LPG	FS_B1	Bare	1548
C	LPG	EX_C4	Coated	1558
C	LPG	ARC_B3	Bare	1568
C	LPG	ARC_C3	Coated	1571
C	FBG	UV MO, irradiated	Bare	1587
C	FBG	UV Welltech, irradiated	Coated	1565
C	FBG	FS Fibertech, irradiated	Bare	1545

[a]The wavelength indicates the position of the attenuation band for LPGs and of the Bragg wavelength for FBGs for measurements at room temperature.

At each side, the sensors have been bundled together and fixed to the mechanical structures of the IDEP at a distance of roughly 140 cm from the beam pipe, as shown in Fig. 12. Each bundle also includes a pair of conventional temperature and humidity sensors, an NTC and an Honeywell probe respectively. These sensors serve as reference devices during operations.[9]

The optical fibers of the FOS and the electrical cables of the NTC and honeywell reference sensors, are passed through the sealed feedthroughs of the IDEP. From there, they are routed out of the

[8] The ATLAS detector has a cylindrical shape, with the axis of the cylinder corresponding to the LHC beams. The two sides of the cylinder are referred to as side A and side C.

[9] For the Honeywell, this is true at least for the first part of the operations, when the accumulated radiation dose in the bundle is relatively low. At high doses, the Honeywell stop working, as they are not designed with radiation-hard characteristics.

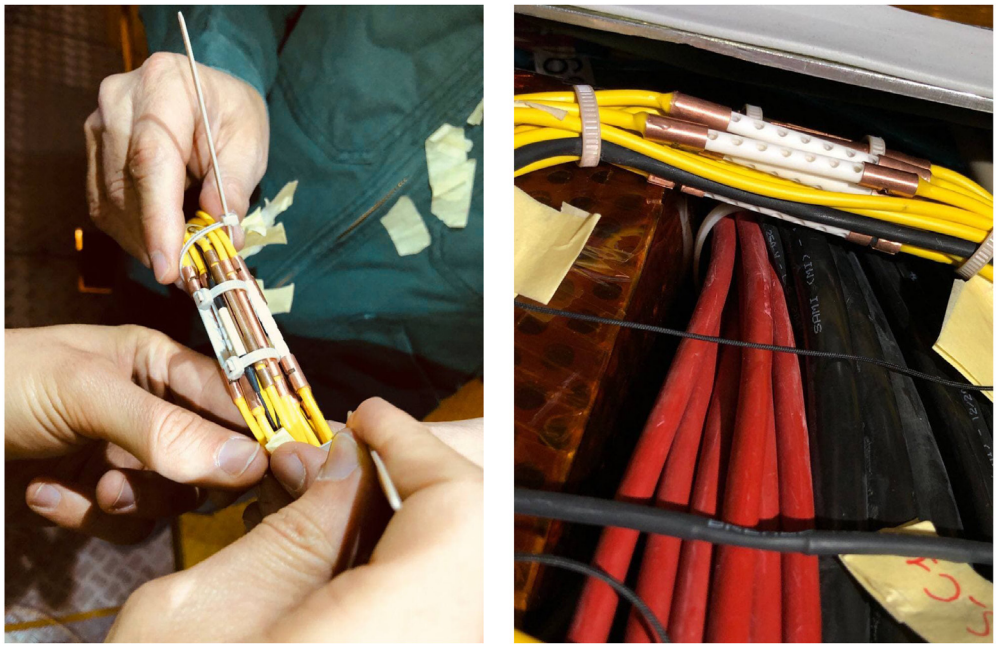

Fig. 12. Installation of the FOS prototypes. Left: FOS bundle. Right: fixation of the bundle inside the IDEP.

ATLAS detector to the floor of the US15 cavern. Here, the fibers are connected to an optical patch panel via LC/APC plugs, while the electrical cables are directly plugged to the readout system of the environmental monitor sensors of the ATLAS SemiConductor Tracker (SCT) subsystem [25]. The signals from the FOS are further carried away from the other side of the patch panel to the readout system installed in the USA15 underground area.

6. Data acquisition system

FOS sensors are readout using interrogation units that inject light into the fibers and record the resulting waveform after transmission through the sensitive pattern. The readout and data acquisition system installed with the ATLAS FOS prototypes makes use of an interrogation unit coupled to an optical switch. This latter component allows to effectively increase the number of available channels.

6.1. Multiplexing

The main concern when dealing with the development of a sensors network based on multiplexed in-fiber grating devices, is the capability of including the highest possible number of independent sensing elements within the available bandwidth of the light source that is used for sensors demodulation. This characteristic is strongly constrained by the interrogation unit that is used to readout the fibers.

In addition, the development of multiplexed LPG-based sensors systems presents more challenges than the one of FBGs. The reason is clear by looking at Fig. 13. FBGs produce narrow peaks in the wavelength pattern, while the LPGs' attenuation bands are sensibly broader. Furthermore, the wavelength shifts produced by FBGs in relation to temperature/humidity variations are much smaller than those produced by LPGs. These facts imply that, given the same bandwidth of the interrogation unit, the number of LPGs that can be multiplexed within a single array is much smaller than the one for FBGs.

The prototype developed for this study is interfaced to an Hyperion si155 interrogation unit. The operational wavelength range of this device is between 1460 nm and 1620 nm. This bandwidth sets a limit to the number of LPGs that can be connected on the same fiber. From the experimental tests carried out, it has been seen that it is possible to insert two or maximum three LPGs in arrays characterized by resonance dips centered at different wavelengths and having an appropriate spectral separation to avoid cross-talk, in accordance with the shifts of the resonance dips due to changes of temperature and humidity.

On top of in-fiber multiplexing, a further increase of the number of readout points has been achieved as follows. Since the Hyperion si155 unit provides only 4 interrogation channels, the number of sensors that one can install is, in principle, limited to just a few. In order to overcome this limitation, on top of producing multiplexed sensor arrays, we included an optical switch in the data acquisition system. The switch was customized with 2 input channels and 24 output channels, the same bandwidth as the interrogator, SMF28 fibers inside, FC/APC connectors on each port, and an Ethernet interface for user control. Pictures of the full DAQ hardware are shown in Fig. 14. This solution allowed the use of two channels of the interrogator to readout the two FBG arrays on each side, while the other two channels are connected to the two inputs of the switch. Looping over the switch's output channels thus allows to serially read the full set of sensors in both side A and side C. Such a connection scheme is shown in Fig. 15.

6.2. Readout and control software

The structure of the control and readout software of the ATLAS FOS prototype is sketched in Fig. 16. The software, including the API of the optical interrogator, is mostly written in C/C++, with elements of python and bash [26].

Communication with the optical switch is achieved using a Telnet link, while the interrogator unit is controlled via TCP/IP using the C/C++ API's provided by the producer. The readout of the reference sensors is integrated with the ATLAS SCT DAQ, and the measurement points are queried directly from the ATLAS Detector Control System (DCS) database.

The FOS control code works under an initialize–run–finalize scheme. The initialization takes care of loading the configurations for the DAQ settings and the individual settings of the sensors, notably the calibration constants. It also builds the internal pointers according to the channel mapping loaded from the DAQ configuration file. The code then enters an infinite loop where the raw data from each sensor are acquired and processed, and the individual calibrations are applied to produce the readings of temperature and relative humidity. A reading

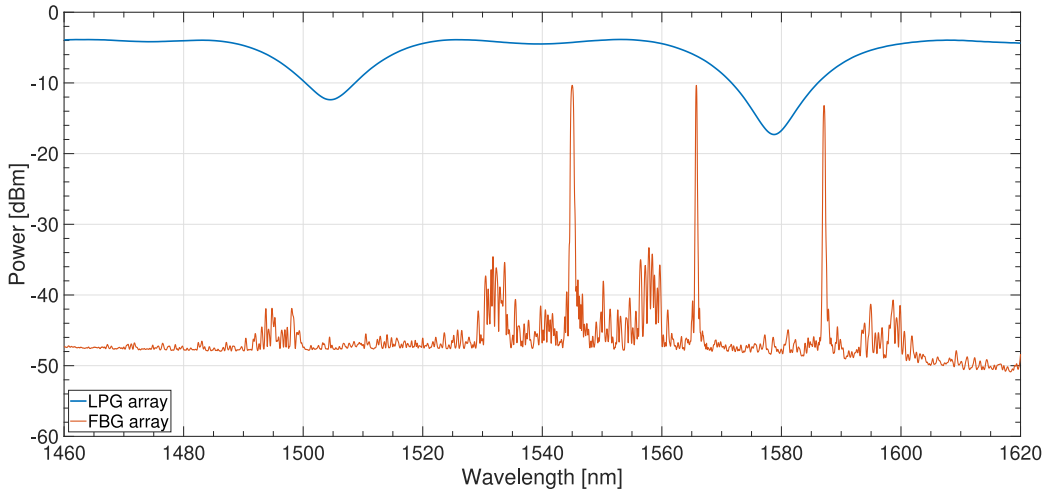

Fig. 13. Comparison between the wavelength spectra of an LPG array (in blue) and an FBG array (in orange). While the two LPG sensors produce two broad attenuation dips, the three FBG sensors display much narrower peaks.

Fig. 14. A picture of the FOS data acquisition hardware installed in the USA15 service room.

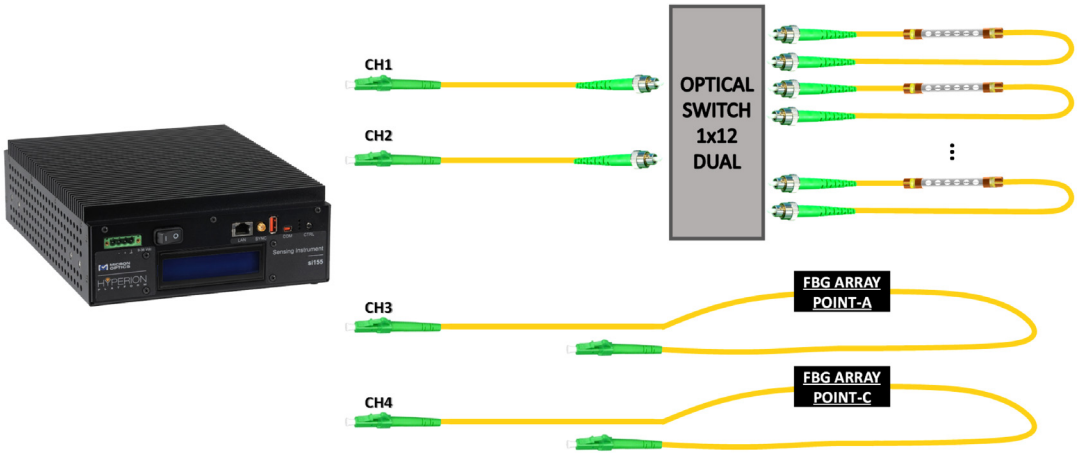

Fig. 15. Schematics of readout elements and their interconnections.

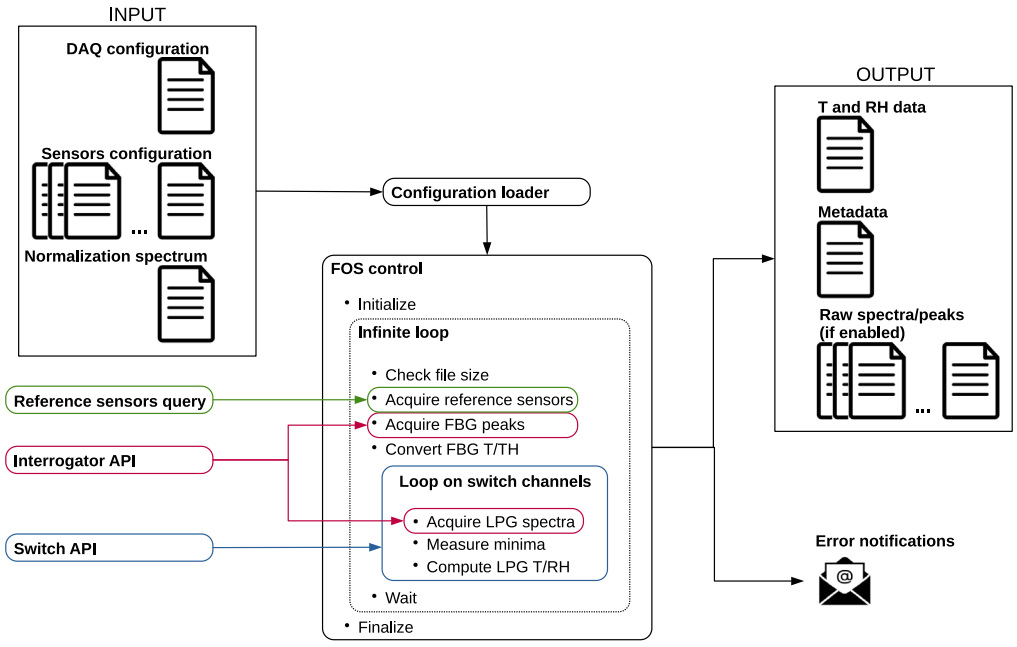

Fig. 16. A sketch of the DAQ and control software.

of the full set of FOS sensors is performed every 10 min, and it lasts for about 20 s, most of the time being taken by the mechanical switching through the channels of the optical switch. At this stage of the project, all the temperature and humidity readings are written to output files, as well as the run's metadata and – upon request from the user – the raw data (full waveforms for the LPGs, peak positions for the FBGs). Current work is in progress to push the readings directly into the ATLAS Detector Control System (DCS) and integrate the FOS data into the ATLAS Finite State Machine (FSM) interface [27].

6.3. Auto (re)calibration

Some of the FOS sensors installed in this prototype system (specifically, the sensors produced via the femtosecond laser and arc discharge techniques) are sensitive to the polarization of the laser. The light source of the Hyperion interrogation unit has a polarization state which, unfortunately, is not guaranteed to be stable in time [28]. Sudden or gradual changes of polarization are therefore possible, and in fact they occur regularly. Experience has shown that, with the current setup, one can rely on a stability period of the order of a few days, after which the sensors that are sensitive to polarization need to be recalibrated to adjust to the new polarization state of the laser.

Recalibration consists in resetting the parameters λ_0, T_0 and RH_0 that enter the conversion Eq. (5) and Eq. (9). As of now, the new values are acquired from the reference NTC and Honeywell sensors. This remains a valid choice at least until the LHC has not delivered a radiation dose that might impair the proper functioning of these devices. Once the sensors will be exposed to significant radiation levels, a re-evaluation of such a choice will be mandatory.

The recalibration of the sensors has been implemented in an automatized routine which reads the new initialization values and stores them in a new set of configuration files. The user's task, apart from launching the recalibration script, consists in simply pointing to the new configuration files for the following data acquisitions. An example of the effect of the recalibration is shown in Fig. 17.

7. Preliminary results

The installation of the sensors inside the ATLAS Inner Detector was accomplished in March 2019. For a first year, the fibers were connected directly to the Hyperion interrogator, which means that a much reduced number of channels were available. Preliminary data were nevertheless useful to understand the behavior of the system and gain experience. In June 2020, the optical switch was installed, allowing for the readout of all the channels in series. However, it was not before the fall of the same year that the full DAQ chain, including the (auto)calibration routine, were finalized. The data reported here thus refer to the period of running beginning as of November 2020, extending up to the time of writing of this paper.

7.1. Temperature readings and polarization effects

The temperature trends recorded in this time span are shown in Fig. 18 for the sensors installed in side A, and Fig. 19 for the sensors installed in side C. In these plots, are also included the readings from the two NTC reference sensors. These results show an overall fair agreement between the reference sensors and the FOS, except for a few isolated cases, notably the LPG FS-B1 in side C. These cases, and the most general deviations from the reference trends, are well explained by polarization effects. One can notice that recalibration cures the dispersion of the trends, at least as long as polarization effects do not take over again. Such effects can be severe on some sensors.

To see the effect of polarization in a cleaner way, one can look at the reading of the same sensor from the two sides of the fiber. This is illustrated in Fig. 20. In this plot, we show the temperature trends of two sensors: LPG FS-B1 (femtosecond laser writing technique, non-axisymmetric), which is sensitive to the laser polarization and LPG EX-B2 (excimer laser writing technique, axisymmetric), which is not. The two sensors are each readout from both sides of the fiber, thus two readings per sensor are displayed. While the sensor produced by excimer laser shows no difference in temperature readings between the two sides of the fiber, the sensor produced by femtosecond laser presents two clearly distinguishable trends at the two sides. Such trends are opposite to each other, which is a clear indication of the effect of the laser polarization.

It is useful to look at the temperature trends of the two LPG sensors alone that were produced by excimer laser. These, against the data from the reference NTCs, are shown in Figs. 21 and 22 for points A and C, respectively. As these sensors are not sensitive to the polarization of the light, they show no sign of miscalibration over time. On top of that, they even seem to provide a higher accuracy in measuring the temperature values, than that of the reference sensors.

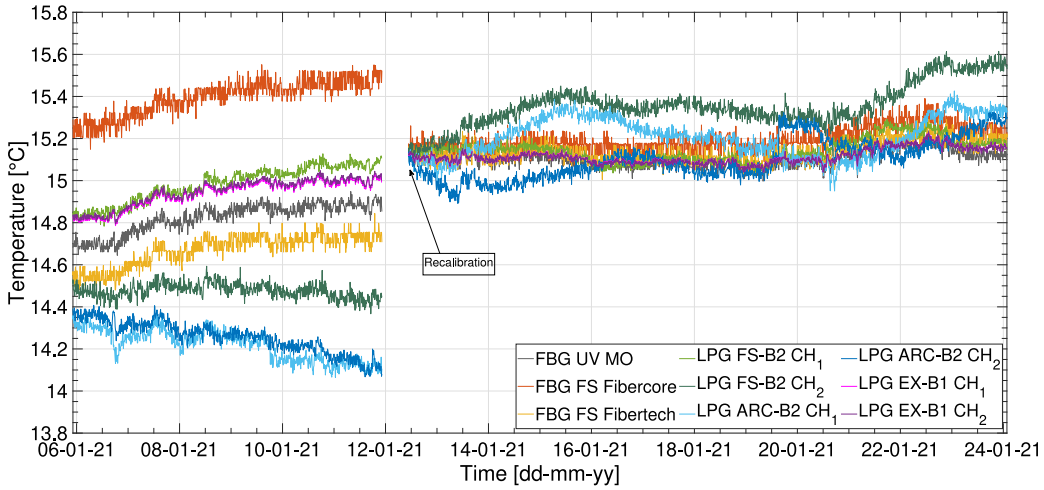

Fig. 17. Temperature trends from a set of sensors. The effect of the auto calibration executed on January 12th 2021 is visible: the temperature drift, caused by a gradual change of the lasers' polarization state, is completely removed.

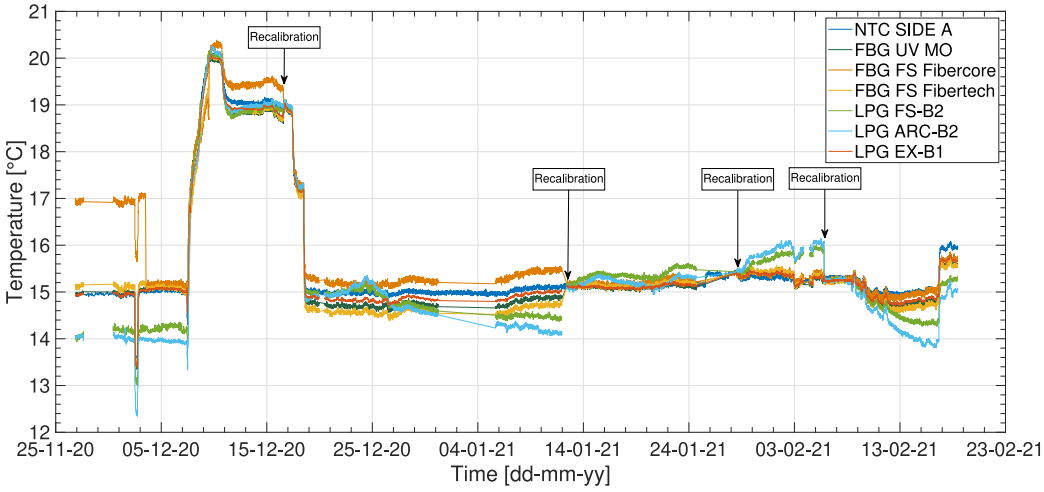

Fig. 18. Temperature trends from the full set of sensors in side A.

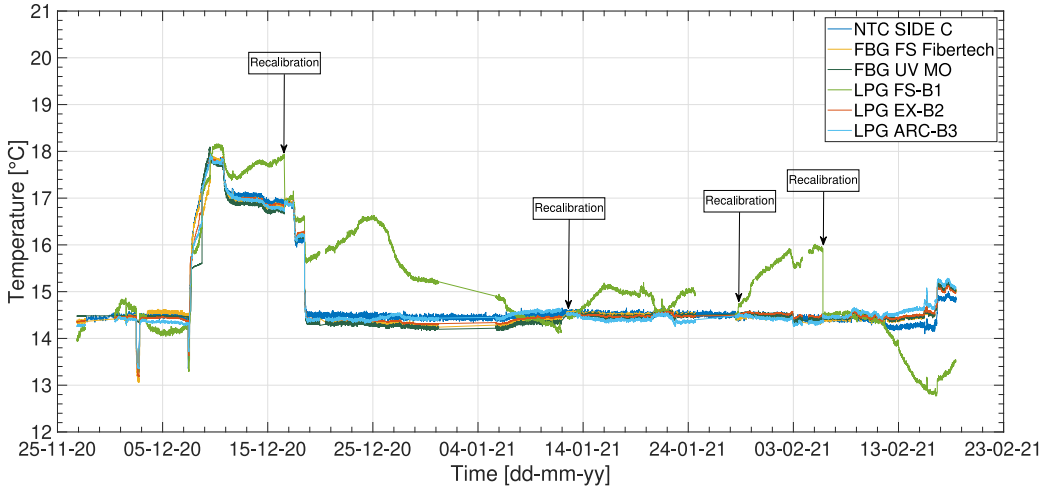

Fig. 19. Temperature trends from the full set of sensors in side C.

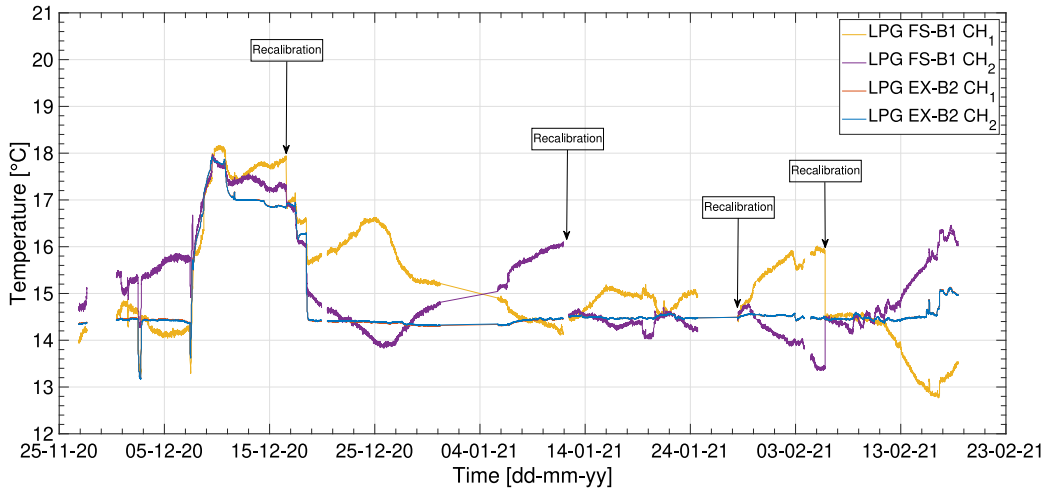

Fig. 20. Comparison between polarization-sensitive and polarization-insensitive LPGs.

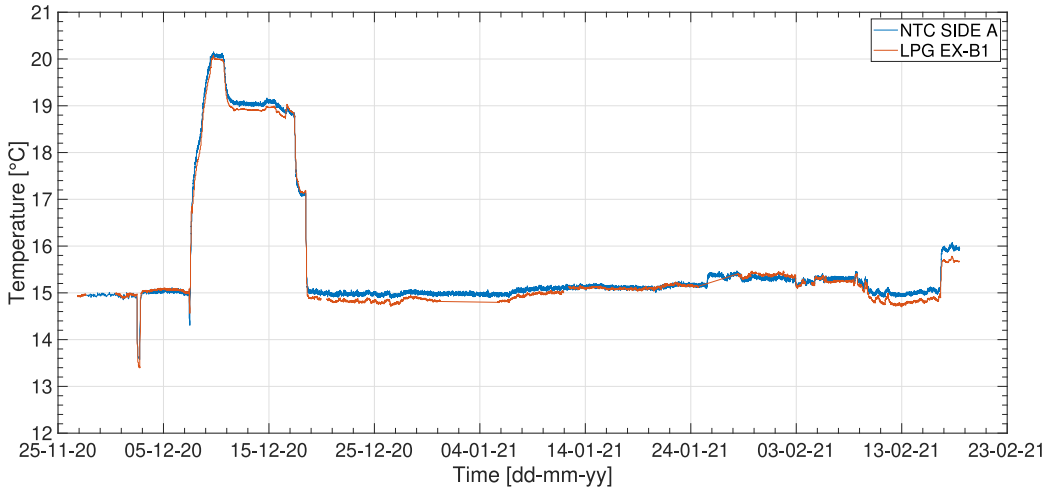

Fig. 21. Comparison between temperature readings from the NTC reference sensor and the LPG FOS written by Excimer laser, in side A.

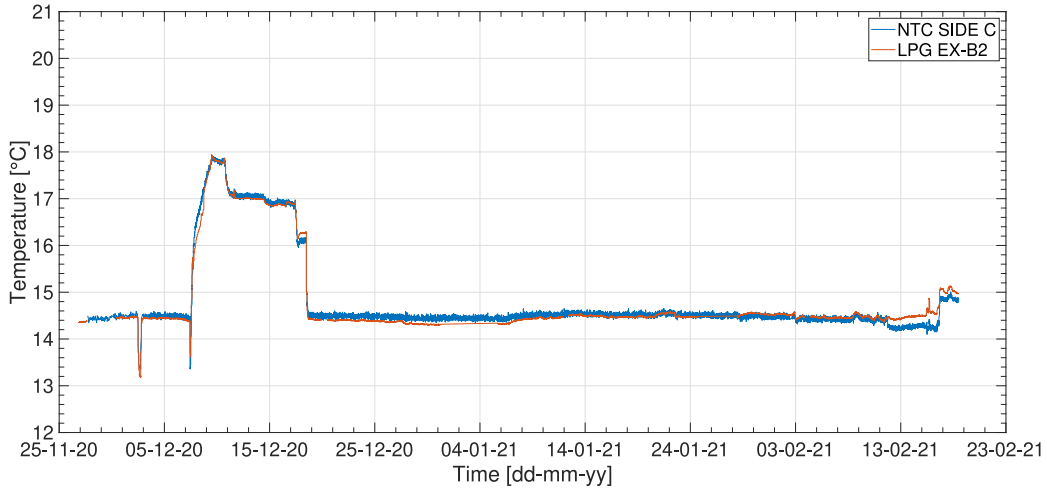

Fig. 22. Comparison between temperature readings from the NTC reference sensor and the LPG FOS written by Excimer laser, in side C.

7.2. Relative humidity readings

Similar observations are valid for the case of the relative humidity measurements. The trends for the full sets of sensors in both side A and C are shown in Figs. 23 and 24. The RH values shown here are calculated using formula (9). The temperature compensation terms appearing in such formula have been calculated with $T_{measured}$ coming from sensors of the same type as the coated FOS. For example, to

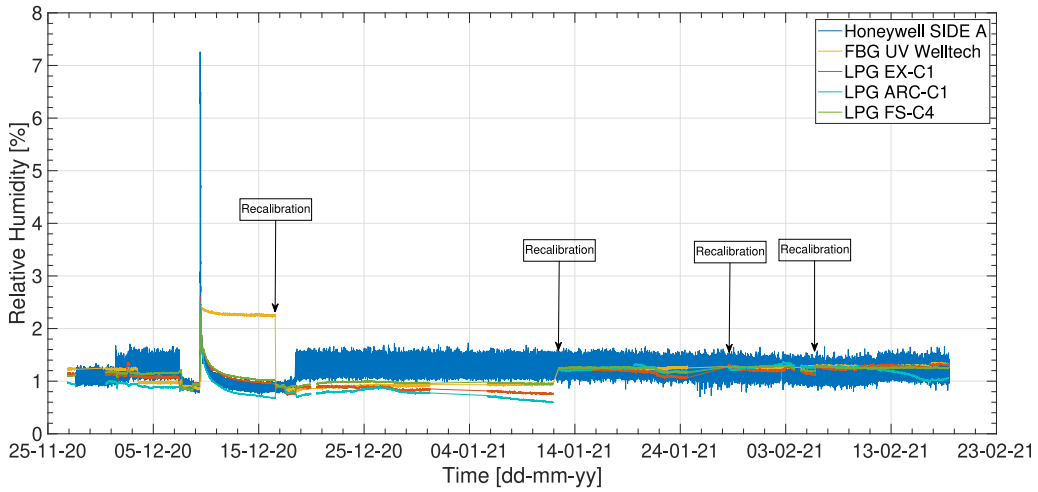

Fig. 23. Relative Humidity trends from the full set of sensors in side A.

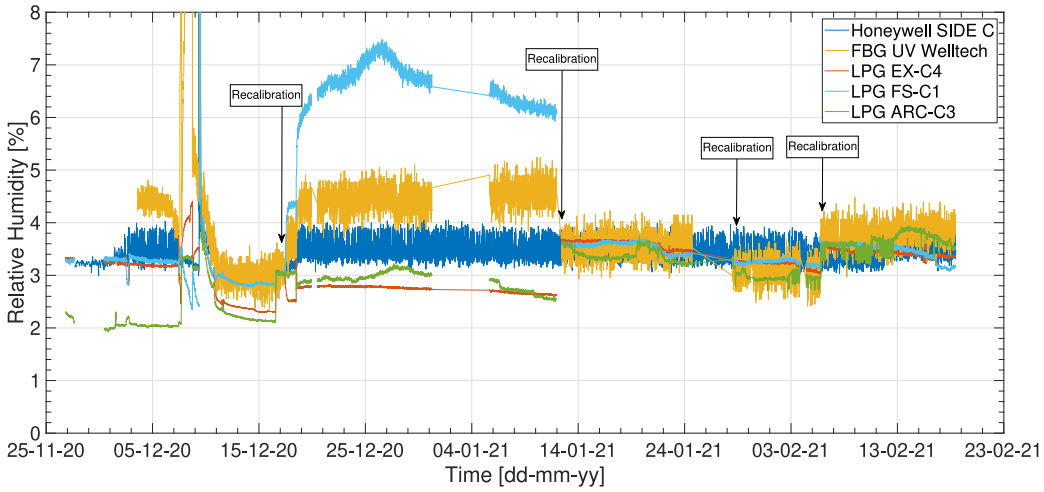

Fig. 24. Relative Humidity trends from the full set of sensors in side C.

calculate the RH value from an ARC-C1 coated sensor, the temperature reading from an ARC-B2 bare sensor has been used.

As in the previous case, FOSs that are sensitive to the polarization of the laser loose calibration with time. However, a new calibration brings the measured values back to the reference RH value. An exception comes again from the LPGs produced by excimer laser, whose trend is isolated in Figs. 25 and 26. These sensors are not sensitive to the polarization of the laser, and thus do not suffer from miscalibration events. Again, and even more strongly than for the T measurements, the RH measurements from the FOS are more accurate than those from the reference Honeywell sensors. In fact, the lower accuracy of these latter is producing visible "jumps" in the RH trends of the FOS. Some of these jumps are strong enough to bring the FOS values outside the noise band of the reference values. However, these jumps are an artifact due to the fact that the (auto)calibration routine takes as reference value for RH, one single reading of the Honeywell sensors, which fluctuates in a much broader range that the average FOS uncertainty. In order to cure this effect, a modification of the calibration code is foreseen, where the reference RH (and possibly also the reference T for the bare sensors) is taken as an average over a few consecutive measurements.

7.3. Dew point monitoring

Following the T and RH measurements, the dew point value was calculated in side A and side C, as shown in Figs. 27 and 28 respectively. In each plot, two dew point traces are compared, one calculated with the reference electrical sensors (Honeywell and NTC) and the other using a bare and a coated LPG as temperature and RH sensors[10]. Both LPGs are written with excimer laser. Since the LPGs are calibrated against the electrical sensors, any calibration error due to the high fluctuations will also affect the dew point calculation. This effect is worsened by the fact that, at low RH levels, a small change in RH produces large changes in the dew point value. Therefore, the use of accurate and precise reference T and RH sensors is crucial.

8. Lessons learned with coated LPGs for humidity monitoring

What was already learnt from operating the network of FBG-based thermo-hygrometers in the CMS experiment, is that these sensors show a limited sensitivity to relative humidity. In part, this is due to the minimal resolution of the interrogation unit, especially at low RH values (RH<5%). Another critical issue of FBGs, is related to the

[10] The discrepancy in the dew point estimations from the two traces, which are visible in the big spike on 7/12/2020 in both Figs. 27 and 28, is a consequence of a sudden temperature and relative humidity change (which are indeed visible in the previous plots). Such a change, which was caused by the cooling system of the ATLAS Inner Detector being set to standby because of a maintenance intervention, happened so fast that the two systems (which are not synchronized) had sampled different temperatures at different times.

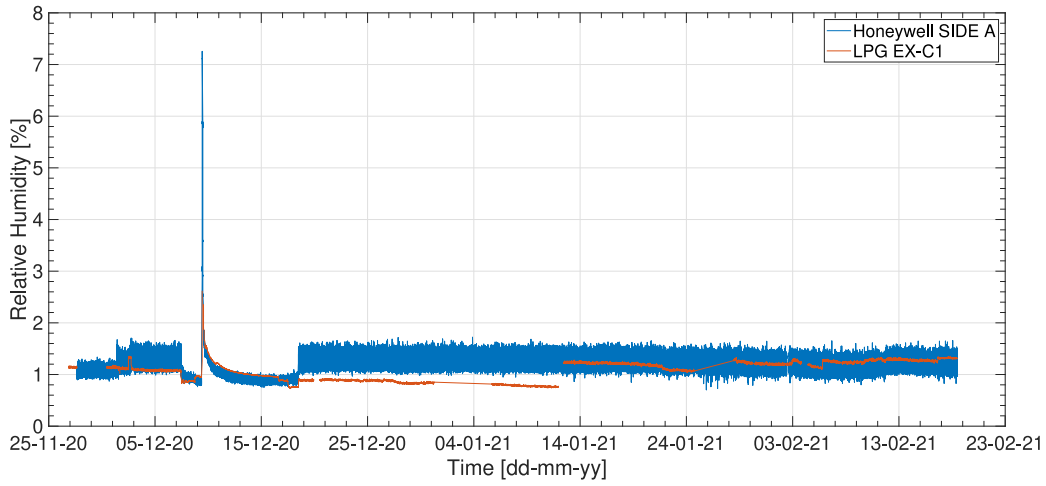

Fig. 25. Comparison between relative humidity readings from the Honeywell reference sensor and the LPG FOS written by Excimer laser, in side A.

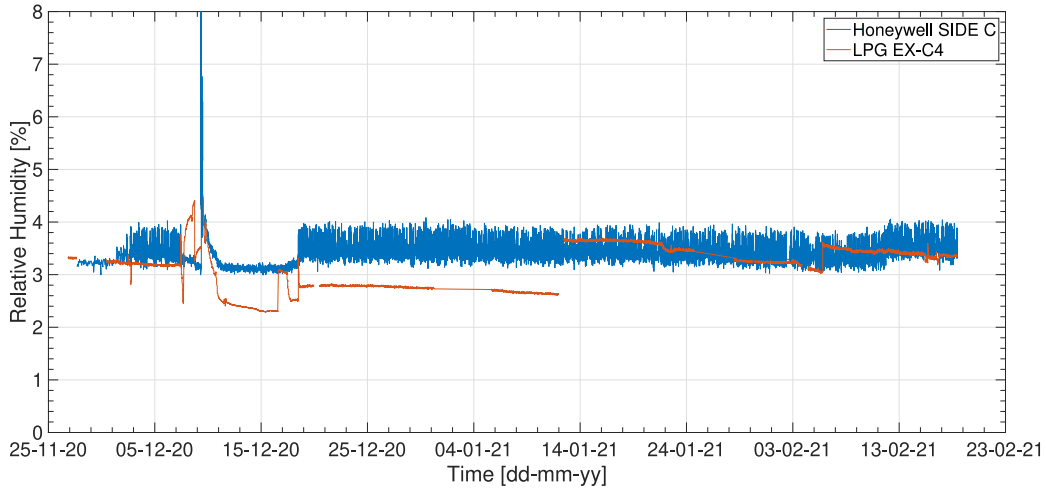

Fig. 26. Comparison between relative humidity readings from the Honeywell reference sensor and the LPG FOS written by Excimer laser, in side C.

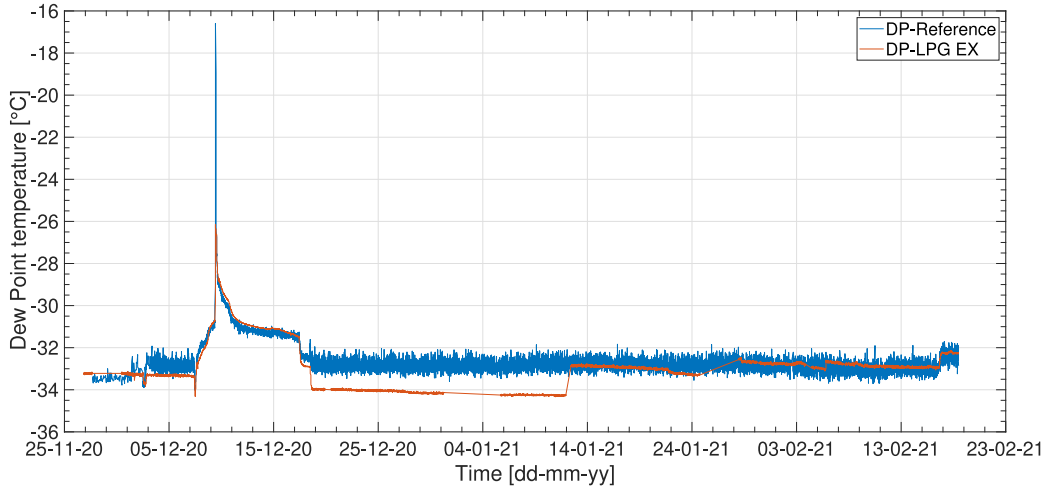

Fig. 27. Comparison between dew point calculated by reference sensors and the LPG FOS written by Excimer laser, in side A.

cross-sensitivity of the coated FBGs to both temperature and relative humidity. To overcome these limitations, a new LPG-based fiber-optic sensor technology has been proposed, which has been installed in the ATLAS Inner Detector.

The first real field installation of LPG-based thermo-hygrometers in the ATLAS experiment confirmed the enormous potential of such devices in harsh environments, especially at low RH levels. Nevertheless, there are some critical aspects to be improved. One of these is

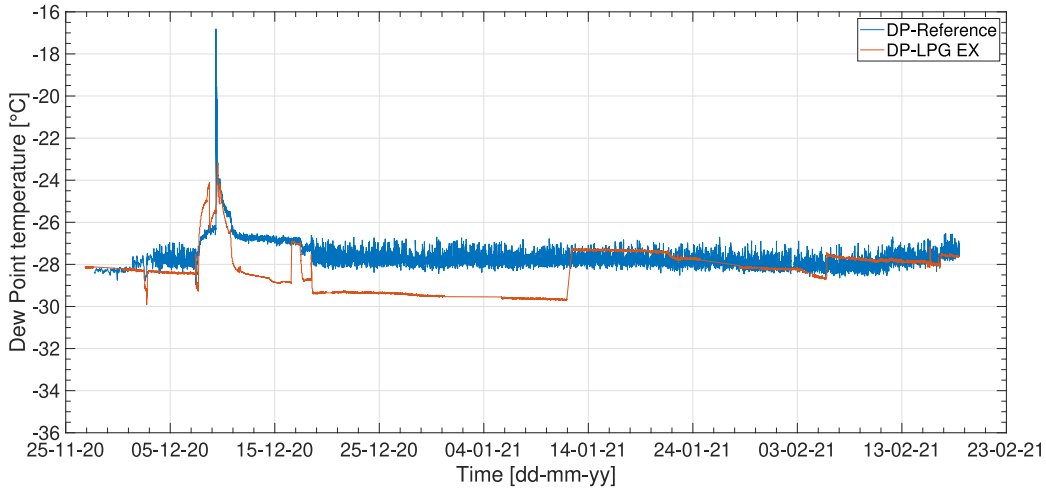

Fig. 28. Comparison between dew point calculated by reference sensors and the LPG FOS written by Excimer laser, in side C.

the manufacturing process of the sensor itself. In fact, as demonstrated by the first data, two categories of installed sensors based on LPG, the ones fabricated through the femtosecond laser and arc discharge techniques, are sensitive to polarization of the laser. This feature is caused by the absence of axisymmetry in the sensor writing process. The use of these sensors in field applications is critical in two ways: first, the unknown polarization of the sensor installed on field does not match the sensor polarization during the pre-characterization phase in the laboratory; second, the sensor looses calibration when the polarization of the light source is unstable, as explained in Section 6.3. One solution to this problem would be to install depolarized optics into the light source. Such solution has not been pursued for this prototype, as it requires a major (and costly) modification of the interrogation unit. For future development, however, the best solution is to move directly to LPGs written with excimer lasers. The excimer-fabricated LPGs included in this prototype are produced by the Optoelectronics group of the University of Sannio. They are fabricated with a fully axisymmetric manufacturing technique that makes these sensors insensitive to polarization variations. As data confirm, this results in an enormous reliability of these devices.

Another critical aspect of this technology is the engineering of a lightweight and small package that would allow one to keep the sensor pre-stressed without inducing undesirable variations due to the package itself. As we saw in the preliminary laboratory tests, the package developed for these prototypes does not fully comply with this requirement. When approaching the edges of the calibration range, some sensors have shown distorted sensitivity caused by unforeseen package effects. These are due to mechanical deformations of the package, caused by the thermal expansion and/or contraction of the materials.

9. Conclusion

The installation of a prototype system based on fiber optic sensors in the ATLAS Inner Detector demonstrates the interest of the high energy physics community towards this new technology for temperature and humidity monitoring in current and future collider detectors. Such system includes FOS of different technologies: FBGs vs LPGs, bare vs coated, and produced with different fabrication techniques. In particular, we demonstrated the feasibility of multiplexing sensors using an external opto-mechanical unit. This enabled us to overcome a typical limitation of LPGs, namely the small number of such sensors that can be arranged in a single-fiber array.

Thanks to the experience we are attaining with this prototype, we will be capable of driving the choice of the best solutions for future applications. In addition, the use of both FBG and LPG-based FOS demonstrates that the two technologies can be used in a hybrid system. For example, FBGs can be installed in areas where accurate monitoring is not required and where RH levels are greater than 10%, while LPGs can be installed in areas where accurate and precise measurement of T and RH levels is desired.

Operation of the prototype system has allowed us to spot a few weak points (e.g. the dependence of the sensitivity of some sensors on the polarization of the light source) and to hypothesize effective solutions for the future.

The restart of the LHC foreseen for mid 2021, and its running during the following years before the next long shutdown, will provide us with a unique test bench to study the behavior of FBGs (together with the CMS experiment) and LPGs (exclusively in ATLAS) against radiation effects.

Declaration of competing interest

The authors declare that they have no known competing financial interests or personal relationships that could have appeared to influence the work reported in this paper.

Acknowledgments

The authors are grateful to the ATLAS management, for having given us the opportunity to install the FOS prototype setup exploiting the opening of the Inner Detector End Plate during the intervention in March 2019. Likewise, we would like to thank all the operators and technicians that have collaborated with us to make this installation possible. Starting from 26 September 2019, E. J. Schioppa is supported by the Italian research grant Programma Operativo Nazionale Ricerca e Innovazione 2014–2020 - Fondo Sociale Europeo, Azione 1.2 ”Attrazione e Mobilitá Internazionale dei Ricercatori” – Avviso D.D. n. 407 del 27/02/2018, code AIM1882733-3.

References

[1] The ATLAS Collaboration, The ATLAS experiment at the CERN large hadron collider, J. Instrum. 3 (08) (2008) S08003, http://dx.doi.org/10.1088/1748-0221/3/08/s08003.

[2] The ATLAS Collaboration, Technical Design Report for the ATLAS Inner Tracker Pixel Detector, Tech. Rep., CERN, Geneva, 2017, URL https://cds.cern.ch/record/2285585.

[3] The ATLAS Collaboration, Technical Design Report for the ATLAS Inner Tracker Strip Detector, Tech. Rep., CERN, Geneva, 2017, URL https://cds.cern.ch/record/2257755.

[4] The ATLAS Collaboration, ITk radiation simulation public results, URL https://twiki.cern.ch/twiki/bin/view/AtlasPublic/RadiationSimulationPublicResults.

[5] The ATLAS Collaboration, ATLAS Pixel IBL: Stave quality assurance, 2014, ATL-INDET-PUB-2014-006.
[6] G. Berruti, Radiation Tolerant Fiber Optic Humidity Sensors for High Energy Physics Applications (Ph.D. thesis), 2015, CERN-THESIS-2015-321.
[7] F. Esposito, A. Srivastava, S. Campopiano, A. Iadicicco, Radiation effects on long period fiber gratings: A review, Sensors 20 (9) (2020) http://dx.doi.org/10.3390/s20092729, URL https://www.mdpi.com/1424-8220/20/9/2729.
[8] G. Berruti, M. Consales, A. Borriello, M. Giordano, S. Buontempo, A. Makovec, G. Breglio, P. Petagna, A. Cusano, A comparative study of radiation-tolerant fiber optic sensors for relative humidity monitoring in high-radiation environments at CERN, IEEE Photonics J. 6 (6) (2014) 1–15.
[9] G.M. Berruti, P. Vaiano, G. Quero, T.F.P.D. Neves, A. Boniello, M. Consales, P. Petagna, A. Cusano, Analysis of uncoated LPGs written in B-Ge doped fiber under proton irradiation for sensing applications at CERN, Sci. Rep. 10 (1) (2020) 1–12.
[10] F. Esposito, R. Ranjan, A. Stăncălie, D. Sporea, D. Neguţ, N. Becherescu, S. Campopiano, A. Iadicicco, Real-time analysis of arc-induced long period gratings under gamma irradiation, Sci. Rep. 7 (1) (2017) 1–9.
[11] F. Esposito, A. Stancalie, C.D. Negut, S. Campopiano, D. Sporea, A. Iadicicco, Comparative investigation of Gamma radiation effects on long period gratings and optical power in different optical fibers, J. Lightwave Technol. 37 (18) (2019) 4560–4566.
[12] The CMS Collaboration, The CMS experiment at the CERN LHC, J. Instrum. 3 (08) (2008) S08004, http://dx.doi.org/10.1088/1748-0221/3/08/s08004.
[13] G.M. Berruti, et al., One year of FBG-based thermo-hygrometers in operation in the cms experiment at CERN, 2016, JINST 11 P03007.
[14] A.M. Vengsarkar, P.J. Lemaire, J.B. Judkins, V. Bhatia, T. Erdogan, J.E. Sipe, Long-period fiber gratings as band-rejection filters, J. Lightwave Technol. 14 (1) (1996) 58–65.
[15] L. Madhavan, M. Chattopadhyay, Temperature and strain sensitivity of long period grating fiber sensor, Int. J. Res. Eng. Technol. 4 (2) (2015) 776–782.
[16] A. Singh, D. Engles, A. Sharma, M. Singh, Temperature sensitivity of long period fiber grating in SMF-28 fiber, Optik 125 (1) (2014) 457–460.
[17] M. Consales, G.M. Berruti, A. Borriello, M. Giordano, S. Buontempo, G. Breglio, A. Makovec, P. Petagna, A. Cusano, Nanoscale TiO_2-coated LPGs as radiation-tolerant humidity sensors for high-energy physics applications, Opt. Lett. 39 (2014) 4128–4131.
[18] S. Girard, A. Morana, A. Ladaci, T. Robin, L. Mescia, J.-J. Bonnefois, M. Boutillier, J. Mekki, A. Paveau, B. Cadier, E. Marin, Y. Ouerdane, A. Boukenter, Recent advances in radiation-hardened fiber-based technologies for space applications, J. Opt. 20 (9) (2018) 093001, http://dx.doi.org/10.1088/2040-8986/aad271.
[19] A. Gusarov, S. Hoeffgen, Radiation effects on fiber gratings, IEEE Trans. Nucl. Sci. 60 (2013) 2037–2053, http://dx.doi.org/10.1109/TNS.2013.2252366.
[20] A. Cusano, A. Iadicicco, P. Pilla, L. Contessa, S. Campopiano, A. Cutolo, M. Giordano, Mode transition in high refractive index coated long period gratings, Opt. Express 14 (1) (2006) 19–34.
[21] F. Esposito, A. Stăncălie, R. Ranjan, D. Neguţ, S. Campopiano, D. Sporea, A. Iadicicco, Gamma radiation effects on long period gratings and transmitted power in different optical fibers: towards dosimetry applications, in: 26th International Conference on Optical Fiber Sensors, Optical Society of America, 2018, p. TuE85, http://dx.doi.org/10.1364/OFS.2018.TuE85, URL http://www.osapublishing.org/abstract.cfm?URI=OFS-2018-TuE85.
[22] A. Stăncălie, D. Sporea, D. Neguţ, F. Esposito, R. Ranjan, S. Campopiano, A. Iadicicco, Long period gratings in unconventional fibers for possible use as radiation dosimeter in high-dose applications, Sensors Actuators A 271 (2018) 223–229, http://dx.doi.org/10.1016/j.sna.2018.01.034, URL https://www.sciencedirect.com/science/article/pii/S0924424717316710.
[23] A. Stancălie, F. Esposito, R. Ranjan, P. Bleotu, S. Campopiano, A. Iadicicco, D. Sporea, Arc-induced long period gratings in standard and speciality optical fibers under mixed neutron-gamma irradiation, Sci. Rep. 7 (1) (2017) 15845, http://dx.doi.org/10.1038/s41598-017-16225-4.
[24] T. Yeo, T. Sun, K. Grattan, D. Parry, R. Lade, B. Powell, Characterisation of a polymer-coated fibre bragg grating sensor for relative humidity sensing, Sensors Actuators B 110 (1) (2005) 148–156.
[25] J. Jackson, The ATLAS semiconductor tracker (SCT), Nucl. Instrum. Methods Phys. Res. A 541 (1) (2005) 89–95, http://dx.doi.org/10.1016/j.nima.2005.01.043, URL https://www.sciencedirect.com/science/article/pii/S0168900205000550, Development and Application of Semiconductor Tracking Detectors.
[26] E.J. Schioppa, L. Scherino, FOSControl, URL https://gitlab.cern.ch/schioppa/foscontrol.
[27] K. Lantzsch, et al., The ATLAS detector control system, J. Phys. Conf. Ser. 396 (1) (2012) 012028, http://dx.doi.org/10.1088/1742-6596/396/1/012028.
[28] Micron Optics, Technical Note 1108, URL https://lunainc.com/sites/default/files/assets/files/resource-library/TN1108_x55_Depolarized_Laser_Option.pdf.